RSC Advances

PAPER

View Article Online
View Journal | View Issue

Cite this: *RSC Adv.*, 2020, **10**, 15573

Dual stimuli-responsive lanthanide-based phosphors for an advanced full-color anti-counterfeiting system†

Tianlin Wang,[a] Xiangyi Ji,[a] Zhanhui Tao,[a] Xiao Zhou,[a] Zhe Hao,[a] Xinke Wang,[a] Xia Gao,[a] Shuo Wang*[b] and Yaqing Liu *[ac]

Received 19th February 2020
Accepted 13th April 2020

DOI: 10.1039/d0ra01594f

rsc.li/rsc-advances

Dual stimuli-responsive lanthanide (Ln)-based phosphors were prepared for constructing a multi-level full color anti-counterfeiting system. The encrypted information can be visually read out under UV irradiation. Further triggered by water, not only are the fluorescence colors changed, but so are the patterns of the encrypted information. The Ln-based phosphors can be cost-effectively prepared in a simple way, presenting great potential application in constructing an advanced anti-counterfeiting system with a convenient authentication assay.

Counterfeiting in numerous fields has become a big concern all over the world. Not only can tremendous loss in economy be caused by counterfeited items such as documents, banknotes, and luxury products, but devastating consequences for an individual, for example, injury, disease, or even death, can also be caused by counterfeited machinery parts or pharmaceuticals.[1–3] Therefore, developing anti-counterfeiting techniques such as barcodes, watermarks, and box seals has drawn ever increasing attention.[4–6] However, most of the assays are easily cloned due to their predictable and fixed encoding mechanisms. It is still a great challenge to construct advanced anti-counterfeiting techniques to improve the level of security.

In recent decades, fluorescence-based materials including semiconductor nanocrystals, carbon dots, metal nanoclusters, up-conversion nanoparticles, and lanthanide-based (Ln-based) materials have been utilized in extensive anti-counterfeiting fields, where the colorful emissions of the fluorophores are considered as security elements.[7–10] Fluorescent patterns in banknotes and documents such as birth certification and passport are well-known anti-counterfeiting samples. It is noted that most of information is encoded with single-color fluorescence tags which is not safe enough since it can be feasibly replicated.[11–13] To address the challenge, multicolor or dual-mode anti-counterfeiting systems have been developed to augment the security level.[14–19] Though the anti-counterfeiting systems are superior to those encoded with single-color phosphors, the encoded information still can be decrypted under ultraviolet or infrared irradiation. Chemical or physical stimuli-responsive fluorescent materials provide an alternative way for further augmenting the security level.[20]

Among the fluorescent materials, Ln-based materials arouse a growing interest in construction of anti-counterfeiting owing to their attractive functional properties, such as large stokes shift, sharp-emission luminescence, high pure luminescence, and photostability.[21–23] It is noted that most of the reported Ln-based fluorescent materials are easily quenched by water,[24,25] which limits their practical applications. On the other point, however, the fluorescence quenching by water can be used as advantage in anti-counterfeiting system.[26] In the present investigation, a novel Ln-based material has been feasibly synthesized according to the coordination between DPA (2,6-pyridinedicarboxylic acid) and Ce^{3+}, DPA–Ce, which presents blue emission in ethanol while not in water. By further doping guanosine 5′-monophosphate (GMP), the produced complex of DPA–Ce–GMP exhibits bright blue emission even in water, furthermore, DPA–Eu–GMP with red emission in water, ethanol and solid powder is also successfully prepared by simply mixing the DPA, Eu^{3+}, and GMP. To enrich the phosphors for fabrication of anti-counterfeiting tags, solvent-related green-emitting complex of DPA–Tb and the red-emitting complex of DPA–Eu are synthesized according to previous reports with further simplified,[27] both of which exhibit fluorescence in solid powder and ethanol while not in water. By taking advantage of different fluorescence responses of the trichromatic phosphors on water, not only fluorescence color but patterns of the anti-counterfeiting tags are changed under assistance of water, augmenting security level for information protection.

[a]*State Key Laboratory of Food Nutrition and Safety, College of Food Engineering and Biotechnology, Tianjin University of Science and Technology, Tianjin 300457, P. R. China. E-mail: yaqingliu@tust.edu.cn*

[b]*Tianjin Key Laboratory of Food Science and Health, School of Medicine, Nankai University, Tianjin, 300071, P. R. China. E-mail: wangshuo@nankai.edu.cn*

[c]*Beijing Advanced Innovation Center for Food Nutrition and Human Health, Beijing Technology and Business University, Beijing 100037, P. R. China*

† Electronic supplementary information (ESI) available. See DOI: 10.1039/d0ra01594f

As is known that DPA can offer oxygen atoms of the carboxyl group and nitrogen atoms of the pyridine ring and is usually used as remarkable "antenna" for coordinating with Ln(III) to prepare green and red phosphors while seldom for preparing Ln-based blue phosphors.[28–30] Herein, the blue-emitting DPA–Ce is feasibly prepared by first blending DPA and Ce^{3+} in ethanol and then exposing the mixture under UV lamp irradiation (302 nm, 60 W) for 20 min (Fig. 1A). The formation of DPA–Ce is confirmed by its X-ray photoelectron spectroscopy (XPS) (Fig. 1B) that binding energy peaks at 285 eV, 400 eV and 532 eV are attributed to the character of O1s, N1s, and C1s from DPA. The feature binding energy peaks of $Ce3d_{5/2}$ at 886 eV and $Ce3d_{3/2}$ at 904 eV are correspondingly detected.[31,32] The X-ray diffraction (XRD) patterns of pure DPA show the typical peaks with high intensity, while no strong diffraction peak can be seen from the XRD pattern for the DPA–Ce (Fig. S1†), indicating that the crystallinity is lost after chemical coordination with Ce^{3+}. The results indicate the successful preparation of DPA–Ce. To elucidate the fluorescence emission mechanism of the DPA–Ce, a series of control experiments were implemented. As illustrated in Fig. 1A, DPA exhibits dim fluorescence (a), which has no change after being irradiated by UV light (b). No obvious fluorescence signal is monitored from Ce^{3+} before and after UV irradiation for 20 min (c and d). The mixture of DPA and Ce^{3+} also exhibits weak blue emission before UV induction (e). Interestingly, the blue emission is significantly augmented under continuous UV induction (f) and reaches maximum after being irradiated for 20 min (Fig. S2†). Following the same procedure, the influence of ligand and lanthanide ions for the preparation of blue phosphor are further explored. Meanwhile, no fluorescence emission is monitored if replacing ligand by acid (BOP) or replacing lanthanide ions by Gd^{3+}, Ln^{3+}, or Tm^{3+} (Fig. S3†). The results indicate that the blue emission of DPA–Ce is attributed to the synergistic function of DPA, Ce^{3+}, and UV induction. The augmented emission spectrum of DPA–Ce can be split into two Gaussian peaks with maximum intensity at 402 nm (red-dot curve in Fig. 1A) and 442 nm (black-dot curve in Fig. 1A). The energy difference between the two peaks is about 2000 cm^{-1} and is consist with the characteristic splitting of the two 4f ($2f_{5/2}$ and $2f_{7/2}$) ground levels of Ce^{3+} triggered by spin–orbit interaction.[33,34] Electron in the 4f energy level of Ce^{3+} is firstly pumped into the upper 5d energy level, then non-radiatively relaxes to the lowest 5d energy level,[35] and finally radiatively relaxes to the 4f energy levels, resulting in ligand-centered blue emission (Fig. 1C).[36] The optimized fluorescence emission of DPA–Ce is found at 2 : 1 molar ratio of Ce^{3+}-to-DPA (Fig. S4†). As is well known that red (R), green (G) and blue (B) phosphors are considered as trichromatic substrates to construct full color materials. According to previous reports,[27] phosphors of green-emitting DPA–Tb and red-emitting DPA–Eu are feasibly prepared within 5 min *via* blending DPA with Tb^{3+} (Fig. 1E(a)) or Eu^{3+} (Fig. 1F(a)) in ethanol, respectively. The DPA–Ce, DPA–Tb and DPA–Eu present similar solvent-related fluorescence property that they exhibit fluorescence in ethanol (curve a in Fig. 1D–F, respectively) and phosphate buffer (PB) (curve b in Fig. 1D–F, respectively) while lose their fluorescence in water (curve c in Fig. 1D–F, respectively).

Inspired by previous reports that guanosine 5′-monophosphate disodium (GMP) acts as template for preparation of lanthanide-based fluorescence material.[37] Here, GMP is used to

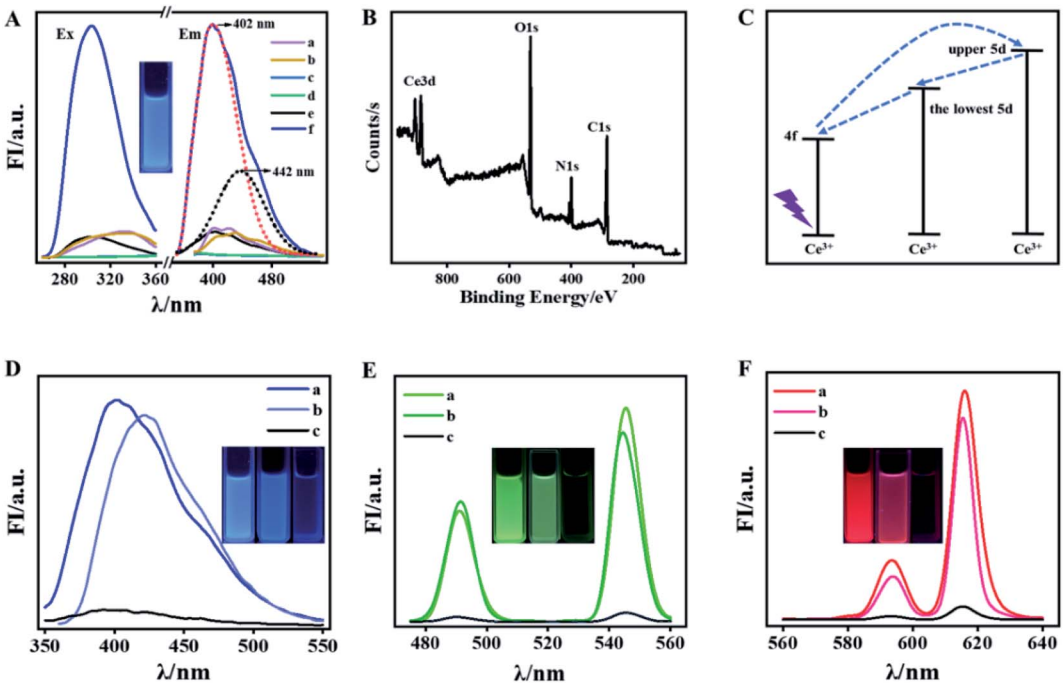

Fig. 1 (A) The excitation and emission spectra of DPA before (a) and after (b) UV induction for 20 min, Ce^{3+} before (c) and after (d) UV induction for 20 min, and DPA–Ce before (e) and after (f) UV induction for 20 min. The Gaussian fitting for the emission of DPA–Ce (red and black-dot curves). (B) X-ray photoelectron spectrum of the DPA–Ce. (C) Diagram of ligand-centred emission mechanism of DPA–Ce. The emission spectra and images of DPA–Ce (D), DPA–Tb (E), and DPA–Eu (F) in ethanol (a), PB buffer solution (b) and water (c).

co-dope with DPA–Ce, DPA–Eu, and DPA–Tb, respectively. It is found that the produced DPA–Tb–GMP loses fluorescence in both ethanol and water (data not shown here), while the produced DPA–Ce–GMP and DPA–Eu–GMP respectively exhibits blue and red emission in both ethanol and water (Fig. 2A and B), which makes it possible for construction of advanced anti-counterfeiting. XPS experiments for element analysis were implemented to validate the successful preparation of DPA–Ce–GMP (Fig. S5A†) and DPA–Eu–GMP (Fig. S5B†). Transmission electron microscopy (TEM) images of DPA–Ce–GMP (Fig. S6A†) and DPA–Eu–GMP (Fig. S6B†) reveal similar 3D network structure which are attributed to the hydrogen bonding and coordinating interaction among DPA, Ln ions, and GMP. The stability of the as-prepared Ln-based phosphors was further explored since stability is a critic factor for phosphors in practical applications. Here, the results represented with DPA–Eu–GMP, DPA–Tb and DPA–Ce–GMP as R-G-B samples (Fig. 2C). The Ln-based R-G-B phosphors can endure continuous high-power UV irradiation (60 W, 2 h). No obvious fluorescence decay is monitored, indicating the outstanding anti-photobleaching property. After being stored in dark for six months, neglectable fluorescence attenuation is detected from the phosphors (Fig. 2D), revealing the excellent ultralong stability. The thermal stability of the phosphors is further investigated by monitoring their fluorescence responses against temperature. The fluorescence remains slight change even the temperature goes up to 150 °C (Fig. 2E), presenting much better temperature quenching resistance than commercial phosphor YAG: Ce^{3+} in consideration of 60% decrease of emission intensity (from 25 to 150 °C).[38]

Once the Ln-based R-G-B phosphors are successfully prepared, full color can be achieved *via* balancing the relative contents of them. With DPA–Eu–GMP, DPA–Tb, and DPA–Ce–GMP as the raw R-G-B phosphors, the prepared materials display colors covering the whole visible range, which can be conveniently distinguished with naked eyes under UV light irradiation (Fig. 3A). According to the fluorescence spectra (Fig. 3B), the corresponding Commission Internationale de L′ Eclairage (CIE) chromaticity diagrams from 1 to 11 are listed in Fig. 3C. The CIE chromaticity coordinates of DPA–Ce–GMP with blue emission are calculated as (0.13, 0.08) and almost the same as those (0.14, 0.08) for the saturated blue phosphor. The as-prepared DPA–Tb with green emission reports CIE coordinates of (0.21, 0.74) closing to those for the saturated green (0.21, 0.71) phosphor. The CIE coordinates are found at (0.65, 0.31) for DPA–Eu–GMP with red emission, which are close to those for the saturated red (0.66, 0.33) phosphors.[39] The fluorescence response is fluently changed from blue to green with increasing relative content of DPA–Tb in its mixture with DPA–Ce–GMP. The increasing of DPA–Eu–GMP in its mixture with DPA–Tb modulates the fluorescence from green to yellow and then orange. The mixtures of DPA–Eu–GMP and DPA–Ce–GMP with different ratio shift the fluorescence emission from red to purple. The corresponding CIE chromaticity coordinates of the generated emission colors distribute in three straight lines, forming a triangle over a wide region to cover full colors. Specially, by finely controlling the relative content of Ln-based R-G-B phosphors at $(DPA–Eu–GMP)_{0.42}(DPA–Tb)_{0.29}(DPA–Ce–GMP)_{0.29}$, white-light emission is achieved with CIE coordinates of (0.31, 0.33) which are quite proximity to the coordinates of

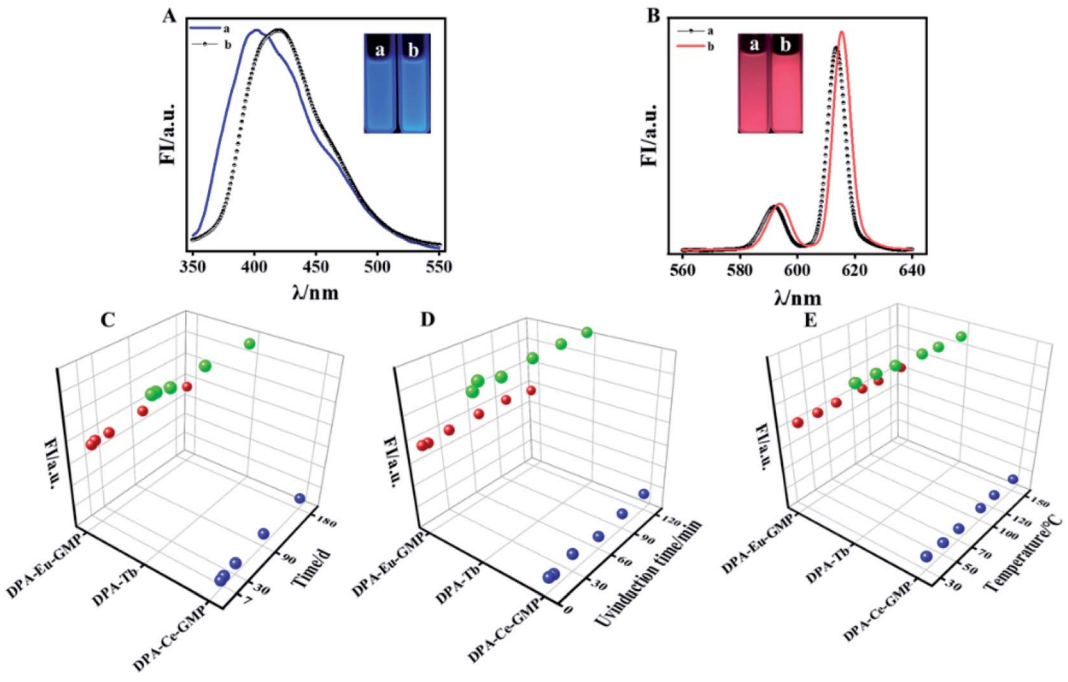

Fig. 2 Emission spectra and fluorescent images of DPA–Ce–GMP (A) and DPA–Eu–GMP (B) in ethanol (a) and water (b). The photo-stability against UV irradiation (60 W, 2 h) (D), the stability up to 180 days (E), and the thermal stability up to 150 °C (F) of the Ln-based phosphors by monitoring the fluorescence intensity of DPA–Eu–GMP at 615 nm, DPA–Tb at 545 nm and DPA–Ce–GMP at 402 nm.

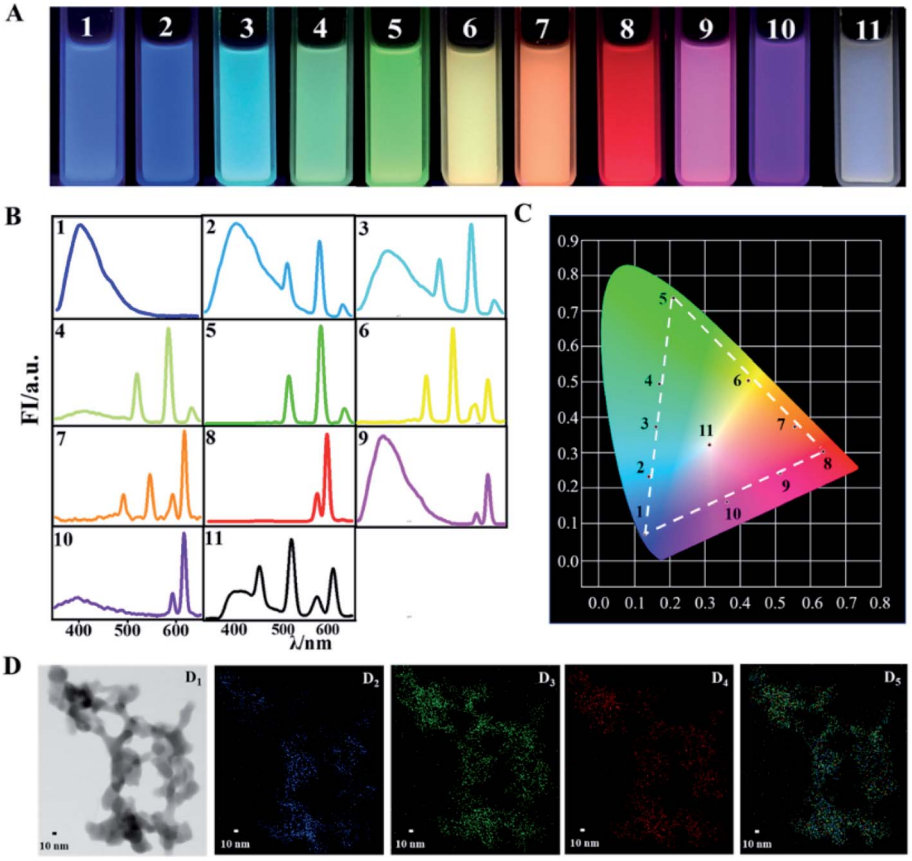

Fig. 3 Images (A), emission spectra (B), and the CIE chromaticity coordinates (C) of full color materials prepared with the Ln-based phosphors in ethanol under the uniform UV light irradiation (302 nm): (1) DPA–Ce–GMP, (2) $(DPA–Tb)_{0.25}(DPA–Ce–GMP)_{0.75}$, (3) $(DPA–Tb)_{0.37}(DPA–Ce–GMP)_{0.63}$, (4) $(DPA–Tb)_{0.75}(DPA–Ce–GMP)_{0.25}$, (5) DPA–Tb, (6) $(DPA–Eu–GMP)_{0.60}(DPA–Tb)_{0.40}$, (7) $(DPA–Eu–GMP)_{0.71}(DPA–Tb)_{0.29}$, (8) DPA–Eu–GMP, (9) $(DPA–Eu–GMP)_{0.37}(DPA–Ce–GMP)_{0.63}$, (10) $(DPA–Eu–GMP)_{0.71}(DPA–Ce–GMP)_{0.29}$, (11) $(DPA–Eu–GMP)_{0.42}(DPA–Tb)_{0.29}(DPA–Ce–GMP)_{0.29}$ under the uniform UV light irradiation (302 nm). (D) TEM image of the white phosphor (D_1) and the elemental mapping diagrams of Ce (D_2), Tb (D_3), Eu (D_4) and the merged diagram (D_5) of D_2, D_3 and D_4.

pure white light (0.33, 0.33). TEM images of the white phosphor (Fig. $3D_1$) reveal similar framework configuration as that of the single portion of phosphors. The elemental mapping diagram (Fig. $3D_5$) discovers that the three elements of Ce, Tb, and Eu (from Fig. $3D_2$ to Fig. $3D_4$, respectively) randomly distribute over the mixture.

The above results strongly prove that the as-prepared phosphors can be excellent R-G-B emission source for construction of full-color anti-counterfeiting tags. Computerized inkjet printing provides a convenient way for pattern construction. Here, the R-G-B inks prepared with DPA–Eu–GMP, DPA–Tb and DPA–Ce–GMP are used to fill a standard R-G-B ink cartridge in a commercial inkjet printer (Deskjet 1111, HP), which can be used to print anti-counterfeiting scheme in large scale and high-throughput inkjet printing. As illustrated in Fig. 4A, the three hollow yellow boxes of the code pattern (4 × 4 boxes) are designed for position recognition of the code, and the other solid colorful boxes are units for information storage, which are invisible under room light (Fig. $4A_1$). Under irradiation of UV light (302 nm), the decrypted colorful fluorescent patterns are found to be identical to the designed code patterns (Fig. $4A_2$). Meanwhile, Fig. 4B shows that the as-prepared GMP, advanced

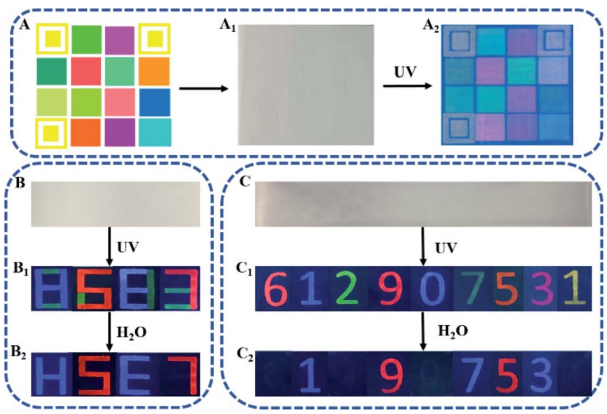

Fig. 4 Images of the coded input pattern (A), the printed pattern on the paper under daylight (B) and UV light (C). Images of written numbers on the paper by using all fluorescent inks under day light (D) and UV light (E). The image of information changing after being triggered by water under UV light (F). Image of the written numbers on the paper under day light (G) and UV light (H). The image of information changing after being triggered by water (I).

anti-counterfeiting tags is further constructed. With DPA–Eu–GMP, DPA–Ce–GMP, and DPA–Tb as R-G-B inks, the information with numbers as model is encoded on a piece of paper, which is directly written with pens loaded fluorescent inks. The numbers are invisible under daylight (Fig. 4B) while display colorful "8683" under UV irradiation (Fig. $4B_1$). Here, the two numbers of 8 are written with blue DPA–Ce–GMP and green DPA–Tb. By controlling the writing position of green ink of DPA–Tb, the two 8 are respectively changed as "H" and "E" after being triggered by water in that the fluorescence of DPA–Tb can be quenched by water. Similarly, the 6 and 3 made of two colors are changed as 5 and 7 in red, Fig. $4B_2$. The decoded information can be changed not only in color but also in configuration that provides an interesting strategy for improving security level. By further blending the as-prepared phosphors with certain ratio, multicolor inks can be prepared to fabricate advanced anti-freighting tags. Written with the prepared inks the numbers can't be observed under day-light (Fig. 4C). Irradiated by UV light, the coded numbers can be directly read (Fig. $4C_1$) that red 6 is originated from DPA–Eu, blue 1 from DPA–Ce–GMP, green 2 from DPA–Tb, red 9 from DPA–Eu–GMP, blue 0 from DPA–Ce, cyan 7 from mixture of DPA–Tb and DPA–Ce–GMP, orange 5 from mixture of DPA–Eu–GMP and DPA–Tb, magenta 3 from mixture of DPA–Eu and DPA–Ce–GMP, yellow 1 from mixture of DPA–Tb and DPA–Eu. Further triggered by water, the numbers of red 6, green 2, blue 0, and yellow 1 disappear since the fluorescence of DPA–Ce, DPA–Eu, and DPA–Tb is quenched by water. Meanwhile, no change is monitored from blue 1 and red 9 since water has no influence on the fluorescence of DPA–Ce–GMP and DPA–Eu–GMP. For the numbers made of mixture of two phosphors, water cause color change of 7 from cyan to blue, 5 from orange to red, and 3 from magenta to blue (Fig. $4C_3$). In this way, the covert information is decoded as colorful "612907531" in the first step and then is converted as "19753" in red (9 and 5) and blue (1, 7 and 3), which provides a new way for authentication purposes in high level. Meanwhile, Fig. S7† shows that the as-prepared phosphors as the RGB fluorescent labeling agents for the visualization of latent fingerprint. Under UV irradiation, the collected finger prints on the glass slide with clear fingerprint lines could be observed after depositing the DPA–Ce–GMP (A_1), DPA–Eu–GMP (A_2), and DPA–Tb (A_3) powder on the glass slide, which consist with the previous reports.[40,41] Therefore, the as-prepared Ln-based phosphors have a widespread potential application in construction of anti-counterfeiting patterns and information encryption.

In summary, three kinds of novel phosphors of DPA–Ce, DPA–Ce–GMP, and DPA–Eu–GMP have been successfully constructed in a quite simple way. By further integrating phosphors of DPA–Eu and DPA–Tb, full color fluorescent materials are prepared to fabricate multicolor anti-counterfeiting system that exhibits advantage over than monocular ones. The security level for information protection is further augmented on the basis of the different fluorescent response of the Ln-based R-G-B phosphors on water. Not only fluorescent colors but also patters of the as-prepared anti-counterfeiting tags are changed under the function of water. Meanwhile, the security patterns can be printed in large scale and high throughput, which makes it very convenience for the preparation of anti-counterfeiting tags. The developed anti-counterfeiting system has advantages of low-cost preparation, simple fabrication procedure, and convenient authentication way. The investigation opens up a new avenue for fabricating advanced anti-counterfeiting system to protect information in high level.

Conflicts of interest

There are no conflicts to declare.

Acknowledgements

This work is supported by the National Natural Science Foundation of China (No. 21575138 and No. 21775108) and Tianjin Science and Technology Project (18PTSYJC00130).

Notes and references

1 B. L. Volodin, B. Kippelen, K. Meerholz, B. Javidi and N. Peyghambarian, *Nature*, 1996, **383**, 58–60.
2 E. Y. H. Hong, C. T. Poon and V. W. W. Yam, *J. Am. Chem. Soc.*, 2016, **138**, 6368–6371.
3 Y. B. Liu, L. Zhou, Y. N. Li, R. P. Deng and H. J. Zhang, *Nanoscale*, 2017, **9**, 491–496.
4 A. F. Smith and S. E. Skrabalak, *J. Mater. Chem. C*, 2017, **5**, 3207–3215.
5 P. Kumar, S. Singh and B. K. Gupta, *Nanoscale*, 2016, **8**, 14297–14340.
6 M. Singh, H. M. Haverinen, P. Dhagat and G. E. Jabbour, *Adv. Mater.*, 2010, **22**, 673–685.
7 T. Song, Q. Q. Yang, H. X. Shi, R. T. Liu, Z. T. Zhang, Z. P. Huang, B. Sun, X. D. Zhang, X. J. Guo, Z. N. Wang, F. Gao, Q. Wang and H. L. Zhang, *Chem. Commun.*, 2019, **55**, 11056–11058.
8 B. Song, H. Y. Wang, Y. L. Zhong, B. B. Chu, Y. Y. Su and Y. He, *Nanoscale*, 2018, **10**, 1617–1621.
9 Z. Gao, Y. F. Han and F. Wang, *Nat. Commun.*, 2018, **9**, 3977.
10 K. Chen, Y. X. Zhang and J. P. Ge, *ACS Appl. Mater. Interfaces*, 2019, **11**, 45256–45264.
11 J. Andres, R. D. Hersch, J. E. Moser and A. S. Chauvin, *Adv. Funct. Mater.*, 2014, **24**, 5029–5036.
12 T. L. Feng, S. J. Zhu, Q. S. Zeng, S. Y. Lu, S. Y. Tao, J. J. Liu and B. Yang, *ACS Appl. Mater. Interfaces*, 2017, **10**, 12262–12277.
13 Y. M. Wang, X. T. Tian, H. Zhang, Z. R. Yang and X. B. Yin, *ACS Appl. Mater. Interfaces*, 2018, **10**, 22445–22452.
14 W. J. Yao, Q. Y. Tian, J. Liu, Q. W. Xue, M. X. Li, L. Liu, Q. Lu and W. Wu, *Nanoscale*, 2017, **9**, 15982–15989.
15 W. W. You, D. T. Tu, R. F. Li, W. Zheng and X. Y. Chen, *Nano Res.*, 2019, **12**, 1417–1422.
16 X. W. Li and Y. C. Hu, *Carbohydr. Polym.*, 2019, **203**, 167–175.
17 X. Chen, W. J. Yao, Q. Wang and W. Wei, *Adv. Opt. Mater.*, 2019, 1901209.
18 W. J. Yao, Q. Y. Tian and W. Wei, *Adv. Opt. Mater.*, 2019, **7**, 1801171.

19 W. J. Yao, Q. Y. Tian, B. Tian, M. X. Li, H. J. Wang, P. Zeng, L. Liu, H. Zheng and W. Wei, *Sci. China Mater.*, 2019, **62**, 368–378.
20 W. Y. Huang, M. Xu, J. J. Liu, J. Y. Wang, Y. B. Zhu, J. Liu and J. T. Zhang, *Adv. Funct. Mater.*, 2019, **29**, 1808762.
21 Y. J. Cui, B. Li, H. J. He, W. Zhou, B. L. Chen and G. D. Qian, *Acc. Chem. Res.*, 2016, **49**, 483–493.
22 X. L. Hu, C. Qin, X. L. Wang, K. Z. Shao and Z. M. Su, *Chem. Commun.*, 2015, **51**, 17521–17524.
23 Y. Jiang, G. Li, W. Che, Y. Liu, B. Xu, G. Shan, D. Zhu, Z. Zhong and M. R. Bryce, *Chem. Commun.*, 2017, **53**, 3022–3025.
24 J. Zhang, Y. Liu, Y. Li, H. X. Zhao and X. H. Wan, *Angew. Chem., Int. Ed.*, 2012, **51**, 4598–4602.
25 T. R. Wang and H. R. Li, *Chem.–Eur. J.*, 2016, **2**, 12400–12405.
26 C. Sun, Z. Y. Gao, H. X. Liu, L. Wang, Y. C. Deng, P. Li, H. R. Li, C. Fan and W. G. Bi, *Chem. Mater.*, 2019, **31**, 5116–5123.
27 H. B. Zhang, X. C. Shan, L. J. Zhou, P. Lin, R. F. Li, E. Ma, X. G. Guo and S. W. Du, *J. Mater. Chem. C*, 2013, **1**, 888–891.
28 J. H. Zhao, S. Wang, S. S. Lu, J. Sun and X. R. Yang, *Nanoscale*, 2018, **10**, 7163–7170.
29 N. Gao, Y. F. Zhang, P. C. Huang, Z. H. Xiang, F. Y. Wu and L. Q. Mao, *Anal. Chem.*, 2018, **90**, 7004–7011.
30 R. Xiong, D. Mara, J. Liu, R. Van Deun and K. E. Borbas, *J. Am. Chem. Soc.*, 2018, **140**, 10975–10979.
31 H. H. Zeng, W. B. Qiu, L. Zhang, R. P. Liang and J. D. Qiu, *Anal. Chem.*, 2016, **88**, 6342–6348.
32 H. H. Zeng, L. Zhang, L. Q. Rong, R. P. Liang and J. D. Qiu, *Biosens. Bioelectron.*, 2017, **89**, 721–727.
33 X. L. Zheng, Y. Liu, M. Pan, X. Q. Lü, J. Y. Zhang, C. Y. Zhao and C. Y. Su, *Angew. Chem., Int. Ed.*, 2007, **46**, 7399–7403.
34 L. Guerbous and O. Krachni, *J. Mod. Opt.*, 2006, **53**, 2043–2053.
35 C. C. Tang, Y. Bando, D. Golberg and R. Ma, *Angew. Chem., Int. Ed.*, 2005, **44**, 576–579.
36 M. J. Dejneka, A. Streltsov, S. Pal, A. G. Frutos, C. L. Powell, K. Yost, P. K. Yuen, U. Müller and J. Lahiri, *Proc. Natl. Acad. Sci. U. S. A.*, 2003, **100**, 389–393.
37 R. R. Gao, S. Shi, Y. J. Li, M. Wumaier, X. C. Hu and T. M. Yao, *Nanoscale*, 2017, **9**, 9589–9597.
38 V. Bachmann, C. Ronda and A. Meijerink, *Chem. Mater.*, 2009, **21**, 2077–2084.
39 Y. Zhou and B. Yan, *Nanoscale*, 2015, **7**, 4063–4069.
40 A. Sandhyarani, M. K. Kokila, G. P. Darshan, R. B. Basavaraj, B. D. Prasad, S. C. Sharma, T. K. S. Lakshm and H. Nagabhushana, *Chem. Eng. J.*, 2017, **327**, 1135–1150.
41 C. Yuan, M. Li, M. Wang, X. Zhang, Z. Yin, K. Song and Z. Zhang, *Chem. Eng. J.*, 2020, **383**, 123076.